A Resonant Band-Pass Filter-Based Facile Recipe for the Estimation of Number Pi

Muhammad Riaz, Hasanah Waqar, Haiqa Maryam
Department of Physics, University of the Punjab, Lahore-54590, Pakistan.
*Correspondence: riaz.physics@pu.edu.pk

Citation | Riaz. M, Waqar. H, Maryam. H, "A Resonant Band-Pass Filter Based Facile Recipe for the Estimation of Number Pi", IJIST, Vol. 08 Issue. 01 pp 240-254, January 2026
Received | December 24, 2025 **Revised |** January 22, 2026 **Accepted |** January 26, 2026 **Published |** January 30, 2026.

In this article, we report an interesting exploration of the basic principles of the Fourier series by using a simple electrical resonant band-pass filter (BPF), driven by a periodic square wave input, and a dual-trace cathode ray oscilloscope (CRO). Here, the BPF circuit is presented as a remarkable Fourier analyzer tool, used to isolate individual frequency components (i.e., the odd harmonics) of the applied square wave. At a fixed resonant frequency (f_0), one can probe the higher-order Fourier components of the square wave, corresponding to lower frequencies of f_0/n. The amplitudes of these odd harmonics can be measured directly from the CRO display or from screenshots captured with a camera. These amplitudes and the corresponding square wave frequencies can then be easily compared with the theoretical prediction of 1/n behavior for n = odd, enabling an engaging and illustrative experiment for students in the laboratory. We also propose the possibility of estimating the value of the famous mathematical constant denoted by the Greek letter π, not only from experimentally measured amplitude values but also from the slope of linearly fitted experimental data. The experimentally determined mean value of π (Pi) was 3.15873, with a total uncertainty of 0.128430. The relative percentage error compared to the accepted value of π (3.14159) was 0.546%, and the percent uncertainty was approximately 0.0003%. Thus, the BPF-based approach yields results consistent with the true value of π within experimental uncertainty. To the best of our knowledge, this paper is unique in presenting such an interesting exploration of the BPF circuit using a CRO while incorporating Fourier components. Finally, in this contemporary age of rapid computation, the suggested experiments provide a valuable addition to physics laboratory experiments involving concepts of Fourier analysis, electrical resonance, BPF circuits, and harmonics.

Keywords: Resonant Band-Pass Filter (BPF); LC Tank Circuit; Fourier Series; Fourier Analyzer; Odd Harmonics; Estimation of the Number Pi (π).

Introduction:

Fourier's discovery (i.e., Fourier series) cannot be overestimated in the modern era, according to which any function that is periodic with a time period T can be described as a summation of sinusoidal waveforms having frequencies that are integral multiples of the fundamental frequency (f_0) [1]. Fourier analysis plays a fundamental role in both physics and mathematics, as demonstrated across a wide range of applications, including the analysis of sound produced by a guitar through standing wave patterns [2], the development of spreadsheet-based instructional tools for laboratory education [3], the examination of Rüchardt's thermodynamic experiment [4], the case of non-linear pendulum [5], the implementation of the Fast Fourier Transform (FFT) as a powerful simulation technique for physics students [6], and the video-based investigation of oscillatory motion in a massive coiled spring [7] among other applications. The concept of a Fourier series (FS) is remarkable and forms the backbone of the experiments presented in this article. Let x(t) be a real-valued periodic square wave function with amplitude V_0 and time period T that satisfies Dirichlet's conditions, as shown in Figure 1(a). The average value over one period for this type of square wave (anti-symmetric) that passes through the origin is zero. The frequency (or amplitude) spectrum obtained by applying the concept of the Fourier series to the square wave is illustrated in Figure 1(b), which relates the amplitudes (A_n) of the harmonic components to their respective frequencies [1].

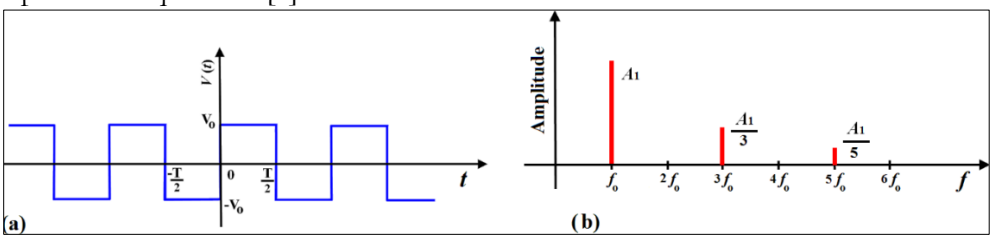

Figure 1. The square wave (anti-symmetric form): (a) temporal behavior, and (b) frequency spectrum.

The Fourier series of a square wave (see Figure 1(a)) contains only odd harmonics, with amplitudes decreasing in a geometric progression, as given below:

$$A_n = \frac{1}{n} A_1 \qquad (n \ \ is\ odd) \quad (1)$$

Here n is an integer. Let us recall the Fourier series, which is written as [1];

$$V(t) = \frac{1}{2} a_0 + \sum_{n=1}^{\infty} a_n \cos(n\omega_0 t) + \sum_{n=1}^{\infty} b_n \sin(n\omega_0 t)$$

Or

$$V(t) = \frac{1}{2} a_o + \sum_{n=1}^{\infty} \left[a_n \cos(n\omega_o t) + b_n \sin(n\omega_o t) \right] \quad (2)$$

Here, $\omega_o \left(= \frac{2\pi}{T_o} = 2\pi f_o \right)$ is called the fundamental frequency and n is the n^{th} harmonic. Moreover, for the equation of the square wave;

$$V(t) = \begin{cases} -V_o, & -\frac{T}{2} < t < 0 \\ V_o, & 0 < t < \frac{T}{2} \end{cases} \quad (3)$$

And

$$V(t + T) = V(t)$$

The coefficients in equation (2) are described as follows. The coefficient a_0 represents the average value of the function V(t) and is actually $a_0=0$, because the average value over one period for a (centered) square wave that passes through the origin is zero see Figure 1(a). The remaining Fourier coefficients can be calculated using the following expression:

$$a_n = \frac{2}{T_0}\int_{-\frac{T}{2}}^{\frac{T}{2}} V(t)\cos(n\omega_0 t)\,dt \quad (4)$$

Furthermore, it is well understood that, for a square wave, the function is odd and therefore cannot contain any cosine terms; consequently, $a_n=0$. Now, let us consider the coefficient b_n as:

$$b_n = \frac{2}{T_0}\int_{-\frac{T}{2}}^{\frac{T}{2}} V(t)\sin(n\omega_0 t)\,dt \quad (5)$$

Solving the above equation (5) by using $\omega_o = \frac{2\pi}{T_o}$, one can easily reach;

$$b_n = \frac{2V_o}{\pi n}\left(1-\cos(n\pi)\right)$$

Or,

$$b_n = \frac{2V_o}{\pi n}\left(1-(-1)^n\right) \quad (6)$$

In short,

$$b_n = \begin{cases} \frac{4V_o}{n\pi} & n\ is\ odd \\ 0 & n\ is\ even \end{cases} \quad (7)$$

The value of b_n represents the desired amplitude of the respective harmonic frequencies. By substituting all coefficients back into equation (2), we obtain:

$$V(t) = \frac{4V_o}{n\pi}\sum_{\substack{n=1 \\ n\ odd}}^{\infty} \sin(n\omega_0 t) \quad (8)$$

This equation applies to the square wave function. Now, we would like to shed some light on the construction of a square wave (a close approximation), which is mathematically given by equation (8) and is, in fact, the sum of an infinite series of sine wave harmonics (n= odd). Figure 2 demonstrates the generation of this square wave using a computer.

The first harmonic (H(1)) and third harmonic (H(3)) in sinusoidal form are shown in Figure 2(a). The dashed green line represents the ideal square wave for reference and represents an ideal square wave. Next, we combined H(1) and H(3) to obtain the resultant H(Total), which appears superimposed (red color) on the ideal square wave. In Figure 2(b), we show H(1), H(3), and fifth harmonic (H(5)) in sinusoidal forms. The resultant H(Total) is also shown, displaying flattened crests and troughs of smaller amplitude than in Figure 2(a). Figure 2(c) depicts the addition of the seventh harmonic (H(7)) to the preceding odd harmonics, producing a smoother resultant waveform. This H(Total) is more flattened than all previous cases, providing a closer approximation to an ideal square wave. These different harmonics correspond to different Fourier components (F.C.) of the same square wave.

Finally, Figure 2(d) presents a combined view of all the resultants from Figures 2(a)–(c), superimposed on the ideal square wave.

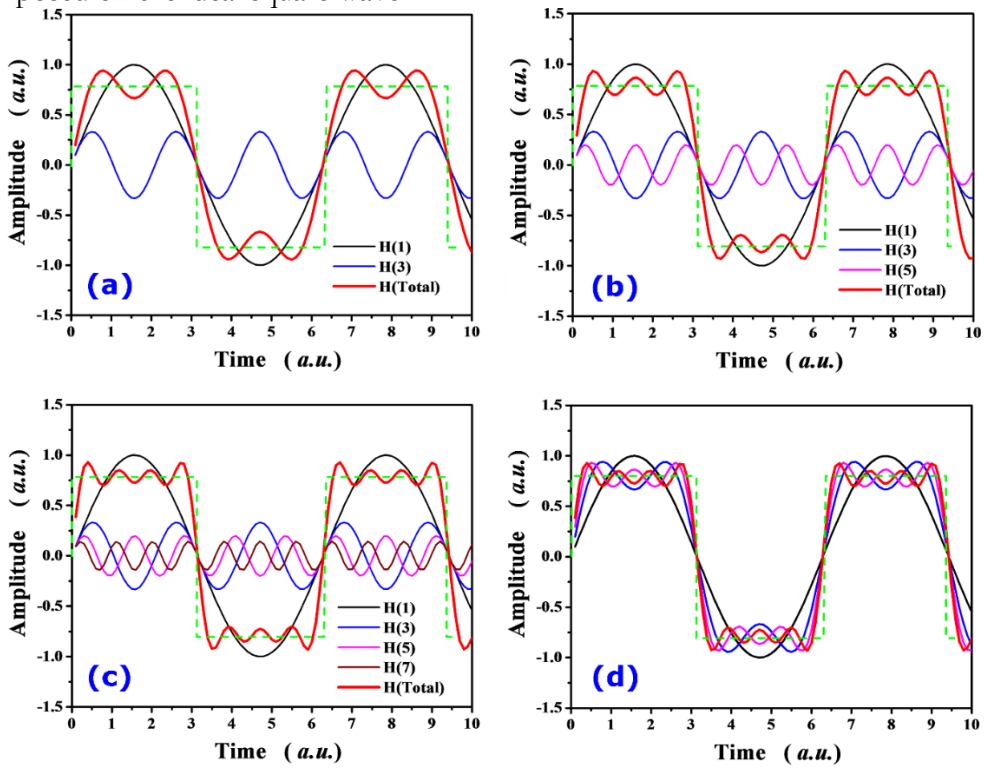

Figure 2. Construction of a square wave (a close approximation). (a) upto third harmonics, (b) upto fifth harmonic, (c) upto seventh harmonics, (d) combined view of all the resultants taken from figure 2 ((a)-(c)) superimposed on ideal square wave (green dotted line). Here, H stands for the term harmonic.

Research Gap:

Experimentation in physics demands a firm understanding of instruments, underlying physical theory, and fundamental principles. Although the fundamental role of Fourier series in physics is well established, comparatively few studies have reported laboratory implementations that employ simple electronic circuitry to integrate theoretical analysis with direct experimental verification within a unified framework. Previous contributions have predominantly focused on domains like waves, oscillations, and acoustics [2][7], thermodynamics [4], mechanics [5], and simulation-based pedagogical approaches [3][6]. This highlights a gap in experimentally accessible simple methodologies, particularly concerning circuit-based strategies for the determination of the value of the mathematical constant π. The present study addresses this need by proposing a compact and experimentally feasible approach that links Fourier theory with electronics, thereby providing a pedagogically valuable and engaging laboratory exercise suitable for physics and engineering courses.

Novelty Statement:

In this article, we describe simple experiments to estimate F.C. using a cathode ray oscilloscope (CRO) assisted resonant band-pass filter (BPF) circuit, utilized as a Fourier analyzer. We also present a unique, experimentally driven approach for determining the value of the number π by using the BPF circuit. In contrast to conventional approaches that rely extensively on mathematical derivations and theoretical formulations, the proposed method extracts π directly from experimentally measured F.C. and simple linear regression analysis, thereby substantially reducing mathematical and computational complexity. By shifting the emphasis from analytical manipulation to measurable circuit behavior, this approach establishes a unique and more accessible practical framework for π estimation. This addresses

an existing gap in practical teaching and laboratory methodologies, where straightforward, circuit-based techniques for determining π are limited. The proposed strategy thus represents a novel and practical alternative that enhances pedagogical practice in physics and engineering education.

Objective:

The primary objective of this study is to determine the value of the mathematical constant π using measurements obtained from a BPF circuit. Sinusoidal waveforms produced by the BPF circuit are recorded from the CRO display, and amplitude measurements are collected multiple times to minimize random error. The value of π was elegantly estimated both from experimentally measured amplitude data captured via CRO screen snapshots and from the slope of linearly fitted experimental data. The resulting values are then compared with the accepted value of π, and the percentage error is computed to evaluate the accuracy of the experimental approach. To the best of our knowledge, this paper is unique in presenting such explorations of a BPF circuit using a CRO while incorporating F.C. and Fourier theory. Hence, the experimental work presented here holds considerable potential as a classroom demonstration or as an engaging experiment in university-level physics laboratories.

The remainder of this article is organized as follows. Section 2 (Materials and Methods) presents the basic circuitry and phenomenology of the BPF circuit. Section 3 details the experimental procedures, including various proposed activities for physics students, along with the corresponding results and discussion. Finally, Section 4 presents the main conclusions.

The Parallel Resonant Band-Pass Filter (BPF) Circuit:

This Section 2 (Materials and Methods) highlights the basic circuitry and phenomenology of the BPF circuit. A systematic experimental workflow chart of the methodology for estimating the value of the number π, outlining the step-by-step procedure, is illustrated in Figure 3. More comprehensive details are outlined in the subsequent sub-sections.

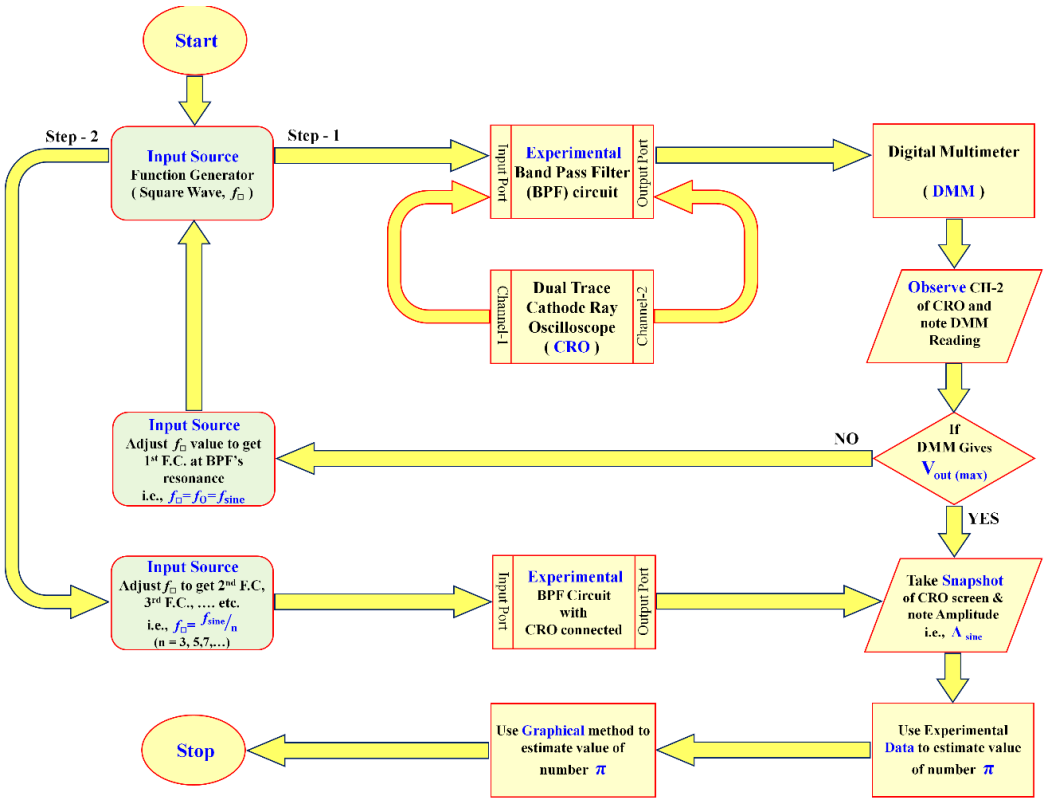

Figure 3. Flow diagram of the experimental procedure, including all steps.

Description: Figure 4 shows the schematic view of the experimental parallel resonant band-pass filter (BPF) circuit utilized as a Fourier analyzer with a fixed resonant frequency (f_o=10 kHz). The other components used in the circuit have the following values: R=15kΩ (or a variable resistor up to 100 kΩ), L=20mH, and C=12.66nF.

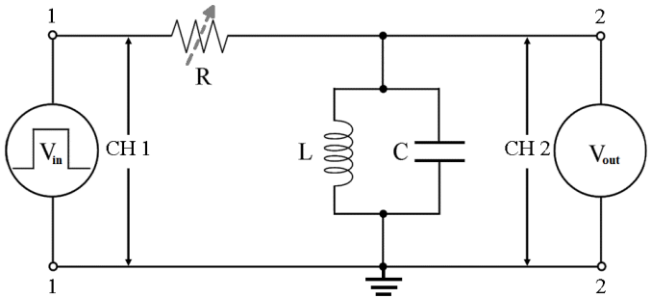

Figure 4. The experimental resonant band-pass filter (BPF) has LC tank circuit values C = 12.66 nF and L = 20 mH. Arrow on the resistor (R) indicates a variable resistor (~100 kΩ); a fixed value of R (~15 kΩ) can also be used.

At the 1,1 port, a a function generator provided a square wave input of fixed amplitude (e.g., 3 V). A dual-trace analog cathode ray oscilloscope (CRO) was used to visualize both input and output waveforms simultaneously. Both channels were set at identical attenuation levels throughout the experiment. Channel 1 (CH-1) was connected to the 1,1 port of the circuit to display a fixed amplitude (e.g., 3 V) on the CRO screen, referred to as A_{square}. This was achieved by adjusting the function generator input voltage Vin.

At the 2,2 port, a digital multimeter (DMM) was employed to record the maximum output voltage (V_{out}) of the circuit with respect to variable frequency values. Additionally, CH-2 of the CRO was connected in parallel with the LC tank at Port 2-2 to display the output sine wave, denoted Asine. A variable resistor (e.g., R=100kΩ) could also be used for fine-tuning the amplitude of the output sine wave on the CRO screen to correspond with the maximum DMM reading, particularly at higher frequencies.

Filtering Action:

RLC resonant circuits are fundamental in electrical and electronics engineering, exhibiting strong frequency-dependent behavior. The series RLC circuit has been extensively studied and forms the basis for analyzing resonance characteristics in more complex configurations. M. Riaz reported an extensive range of periodic attractors obtained experimentally through systematic modification of the component ordering in series LCR-type resonant circuits [8]. Another study [9] showed that the transient and underdamped response of a series RLC circuit can be effectively utilized as a frequency multiplier.

Although the series RLC configuration provides a foundation for understanding resonance, the parallel configuration plays an important role in filter design, allowing circuits to isolate particular frequency components. Let Z_{LC} be the complex frequency-dependent impedance of the LC tank circuit (see Figure 4), which is in series with R. The value of Z_{LC} is given by:

$$Z_{LC} = \frac{X_L X_C}{X_L + X_C} \quad (9)$$

Where $X_L = j\omega L$ and $X_C = \frac{1}{j\omega C}$. Therefore, the complex impedance of the parallel LC branch is given as:

$$Z_{LC} = \frac{j\omega L}{1 - \omega^2 LC} \quad (10)$$

Since resistor R is in series with the parallel LC branch, the total series impedance Z_{Total} is given by:

$$Z_{Total} = R + Z_{LC} = R + \frac{j\omega L}{1-\omega^2 LC} \quad (11)$$

Let us use the voltage divider rule, on the series form of the circuit see Figure 4, according to which, the voltage across any series element is proportional to its impedance relative to the total series impedance. Mathematically:

$$V_{element} = \left(\frac{Z_{element}}{Total\,series\,impedance} \right) V_{total}$$

Here, $V_{out} = V_{LC} = \left(\frac{Z_{LC}}{R + Z_{LC}} \right) V_{in}$ (12)

V_{LC} is the voltage across the parallel LC branch, and at resonance, almost all V_{in} appears across it as Z_{LC} tends to infinity ($Z_{LC} \rightarrow \infty$). Resistor R plays the role of damping and reduces the peak voltage at resonance and broadens the bandwidth. The magnitude of the equation (12) is given by:

$$|V_{out}| = \left(\frac{|Z_{LC}|}{\sqrt{R^2 + |Z_{LC}|^2}} \right) |V_{in}| \quad (13)$$

Using equation (10) in equation (13) and solving, we get:

$$|V_{out}| = \left(\frac{1}{\sqrt{1 + \left(\frac{R(1-\omega^2 LC)}{\omega L} \right)^2}} \right) |V_{in}| \quad (14)$$

This equation (14) is the complex frequency-dependent voltage divider, describing how much of the input voltage appears across the parallel LC branch and what its phase is relative to the source voltage V_{in}. Now, let us define the Quality Factor (Q-factor) of a resonant circuit, which determines how sharply it selects frequencies. Mathematically:

$$Q = \frac{reactive\,energy\,stored}{energy\,dissipated\,per\,cycle} = \frac{1}{R}\sqrt{\frac{L}{C}} = \frac{\omega_o L}{R} \quad (15)$$

And,

$$BW = \Delta\omega = \frac{\omega_o}{Q} \quad (16)$$

The above equations (15) and (16) measure the BPF's selectivity (i.e., high Q), where a higher Q results in a narrower bandwidth and sharper resonance. Simple and straightforward methods for estimating the Q of damped oscillations have been reported in the literature elsewhere [10][11].

Now, the filtering action of the BPF, as illustrated in the generalized frequency response curve for both V_{out} (blue solid line) and I (red dotted line), is shown in Figure 5. In brief, it indicates that V_o is the maximum voltage value corresponding to the resonant frequency (f_o). The frequencies f_1 and f_2 are the two band-limit frequencies corresponding to a voltage value of $0.707V_o$.

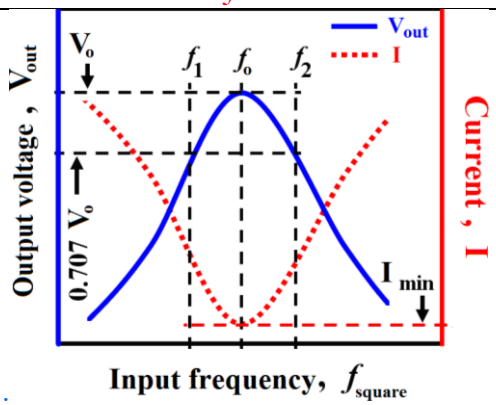

Figure 5. Generalized frequency response curves for parallel resonant BPF. Here, V_o is the maximum value of voltage corresponding to the resonant frequency (f_o). The frequencies f_1 and f_2 are two band limit frequencies.

At very low input frequency ($f_{square} < f_1$), the maximum portion of the input square wave voltage (V_{in}) is dropped across the resistor (R), since the impedance (Z_{LC}) of the LC tank circuit is very low. An increase in f_{square} not only increases Z_{LC} of the tank circuit but also the voltage drops across it (i.e., V_{out}). At f_o, the maximum portion of V_{in} is dropped across the tank circuit as its Z_{LC} reaches a maximum. A further increase in f_{square} beyond f_o decreases Z_{LC} , which ultimately reduces the value of V_{out}. Clearly, when f_{square} increases to f_1, the voltage (V_{out}) rises towards $0.707V_o$, while the current (I) decreases. A further increment in f_{square} (from f_1 to f_o) increases V_{out} from $0.707V_o$ to V_o, and I decreases to its minimum value (I_{min}) at $f_{square} = f_o$. Even further increments in f_{square} (from f_o to f_2) cause V_{out} to decrease from V_o to $0.707\ V_o$, while I increases from I_{min} to its maximum. After $f_{square} > f_2$, the value of V_{out} falls below $0.707\ V_o$, and I continues to increase.

Moreover, the BPF circuit allows the Fourier components (F.C.) present in the square wave input (V_{in}) of frequency f_{square} to pass while filtering out harmonics above f_o, as shown in Figure 6. In fact, we aim to estimate such an F.C. using a CRO-assisted parallel resonant band-pass filter (BPF) circuit employed as a Fourier analyzer (see upcoming Section 3.1). Here, we probe at a fixed frequency (f_o) the higher-order F.C. of the square wave with a lower frequency (f_o /n) via the BPF and a CRO . The magnitude of the F.C., as displayed in sinusoidal form on the CRO screen (inset of Figure 6), is recorded and used for the intended experiments.

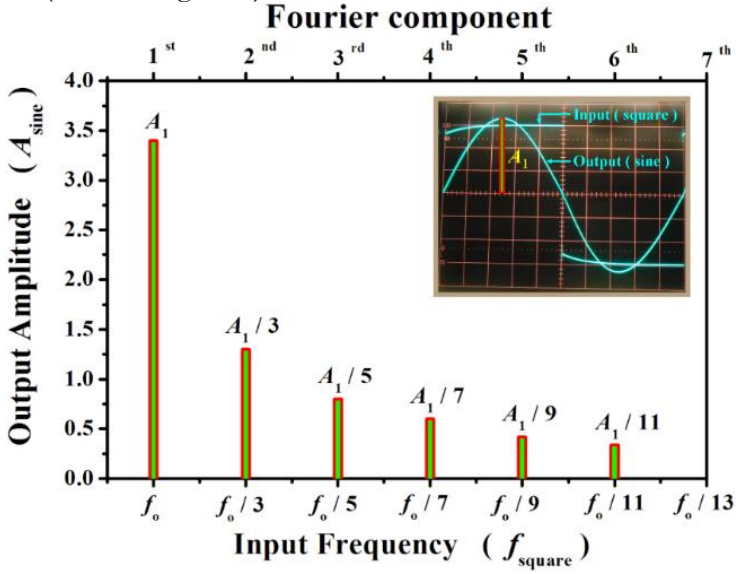

Figure 6. The plot showing output amplitude versus the frequency spectrum. Inset show original image CRO display for A_1.

Purposed Experiments:

Fourier Component (F.C.) Analyzer:

As a first step, f_{square} was increased steadily until the resonance of the circuit was reached (i.e., $f_{square} = f_o = 9950$ Hz). At the 1,1 port of the BPF circuit see Figure 4, the input voltage amplitude was maintained at a fixed value (e.g., 3 V) throughout the experiment. At the 2,2 port of the circuit see Figure 4, CH-2 displayed a low-distortion sine wave on the CRO screen, as shown in the inset of Figure 6. The amplitude of this sine wave ($A_{n(sine)}=A_{1(sine)}$) was recorded from the CRO screen corresponding to the first harmonic (n=1), which appears to be greater than the square wave amplitude (A_{square} or $V_{o(square)}$) because at f_o we have

$$A_{n\,(\sin e)} = \frac{4V_{o\,(square)}}{\pi}.$$

After that, $f_{n(square)}$ was gradually reduced till the detection of another resonance (i.e., second F.C.) at theoretically $f_{3\,(square)} = \frac{f_o}{3}$. This $f_{3(square)}$ together with the value of $A_{3\,(sine)}$ observed from the CRO screen (see Figure 6) is recorded. The above process is repeated for the third F.C. through the sixth F.C. Hence, this BPF circuit is, in essence, a detector for the sub-harmonics (or F.C.) present in the V_{in}.

The experimental results, as CRO screenshots recorded for odd harmonics (n = 1, 3, 5, 7, 9, 11), are shown in Figure 7 (a) to (f), respectively. Shaded regions indicate portions of the waveforms used to calculate the respective amplitudes. Insets show zoomed views of these regions for easier reading of the amplitude values (An(sine)). The value of A_{square} was kept constant at A_{square} =3 Volts (i.e., 3 square boxes on the CRO screen). Here, the observed increasing deviation of higher-order harmonics (see Figure 7) from theoretical predictions can be attributed to several practical system limitations. Firstly, the finite bandwidth of the BPF circuit inherently attenuates higher-frequency F.C., and its Q-factor further modulates their amplitude response. Secondly, intrinsic harmonic attenuation arising due to frequency-dependent losses in passive components, parasitic capacitance or inductance, and skin effect may contribute to the progressive decrease in amplitudes of higher harmonics. Finally, nonlinearities within the experimental setup can introduce distortion, thereby suppressing specific harmonics and inducing phase shifts. A quantitative analysis integrating the above considerations can reconcile experimental findings with theoretical expectations.

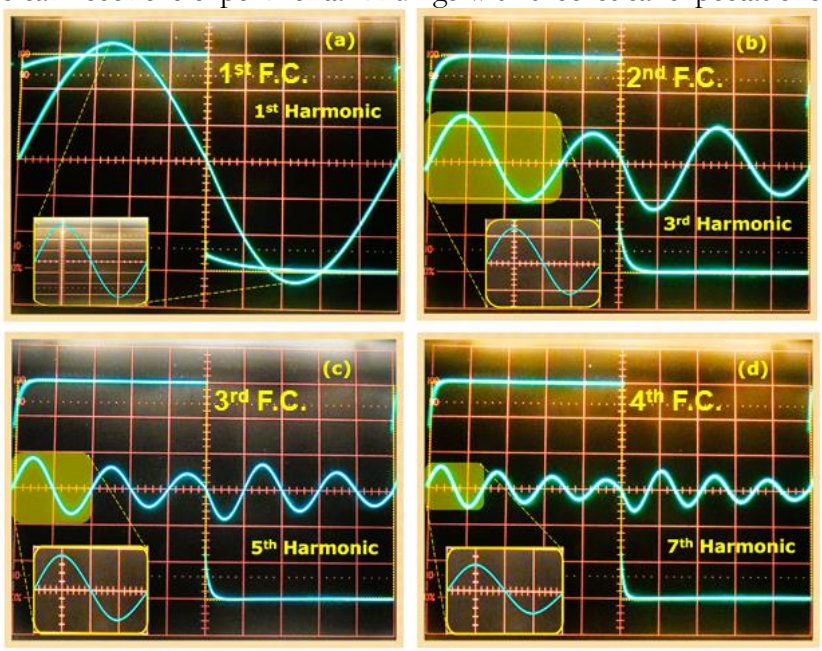

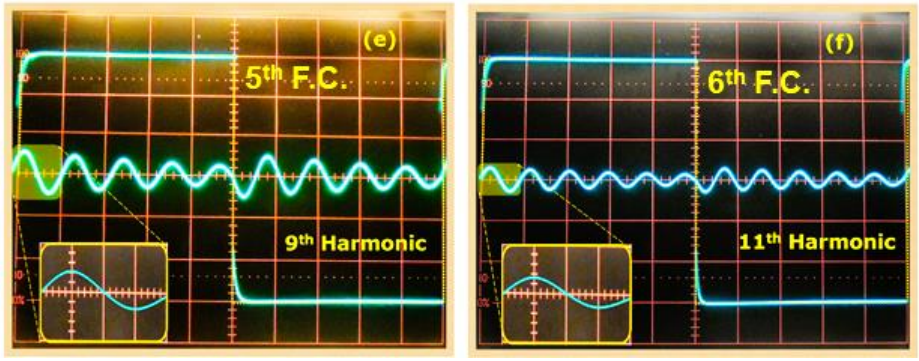

Figure 7. (a) to (f) Screen shots of CRO images taken at odd values of the f_{square} multiplying factor n = 1 to 11, respectively. Here, F.C. stands for Fourier components. The shaded region represents the portion of the wave to be used for the respective amplitude calculation. The inset shows the same shaded region in zoom view for easy amplitude reading. The input was A_{square} = 3 boxes (or Volts).

The main findings obtained from the measurements shown in Figure 7 are tabulated in Table 1. This information will be used for the experiments described in the subsequent sections.

Table 1. Summary of experimental results presented in Figure 7 (with A_{square} = 3 Volts)

Harmonics (*n*)	**Name of Fourier component(F.C.) at f_0 / n**	**Experimental input frequency ($f_{n\,(square)}$) Hz**	f_0 / f_n *(square)*	**Output Amplitude ($A_{n(sine)}$) Volts**	$A_{1\,(sine)}) / A_{n\,(sine)}$	$4\,A_{(square)}) / A_{n\,(sine)}$	Π (by equation (17))
1	1st	9950	1.00	3.70	1.00	3.24324	3.24324
3	2nd	3430	2.90	1.26	2.94	9.52381	3.17460
5	3rd	2052	4.85	0.75	4.93	16	3.2
7	4th	1470	6.77	0.55	6.73	21.81818	3.11688
9	5th	1145	8.69	0.43	8.61	27.90698	3.10078
11	6th	930	10.70	0.35	10.57	34.28571	3.11688

Frequency and Amplitude Spectra:

A plot of frequency or amplitude versus harmonic number is called the frequency spectrum or amplitude spectrum of the square wave, respectively. This experiment uses the experimental data provided in Table 1 (up to the sixth column) to help students easily understand the basic concepts of histograms by plotting the frequency spectrum (i.e., column 1 versus column 3) or amplitude spectrum (column 1 versus column 5) of the given BPF circuit. In Figure 8, we present our experimental results in the form of the frequency spectrum (Figure 8 (a)) and amplitude spectrum (Figure 8 (b)).

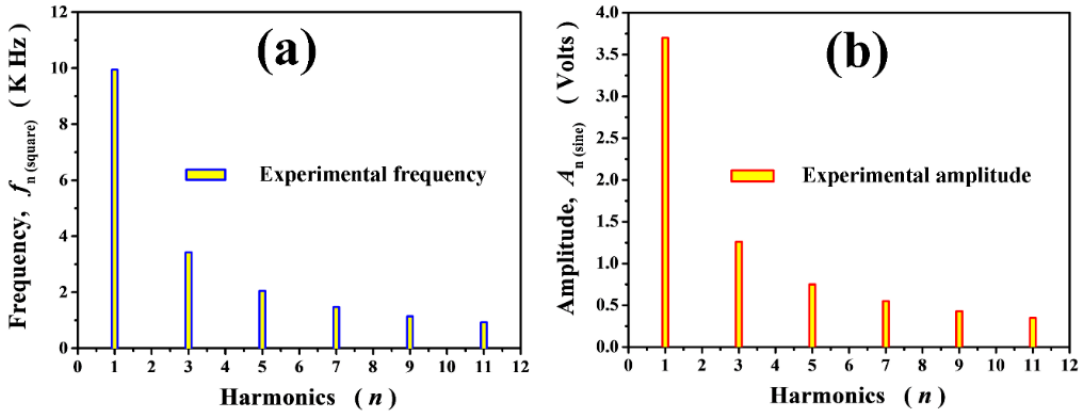

Figure 8. Experimental results of: (a) frequency spectrum, and (b) amplitude spectrum.

The students may measure the amplitudes ($A_{n\ (sine)}$) either by direct observation of the CRO screen (by counting the number of its boxes) or by capturing an image of the waveform with their smartphone camera for a more accurate readout of the respective amplitudes ($A_{n\ (sine)}$) by using the zooming feature of the smartphone. These measured amplitudes can then be compared with the theoretical 1/n behavior for odd n.

In addition, the ratios columns (columns 4 and 6) of the above Table 1 could be plotted against the harmonic numbers (n) given in column 1. A graphical comparison of these results is depicted in Figure 9, which confirms fairly good agreement with the theoretical line (plotted n versus n). Besides, these experimental ratios show a systematic increase in deviation (from the theoretical line) with increasing harmonicity.

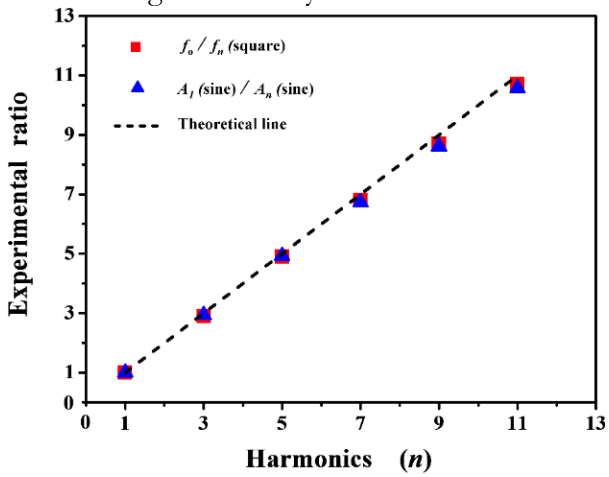

Figure 9. The experimental ratios of frequency (red solid squares) and amplitude (blue solid triangles) are plotted against harmonic number (n) and then compared with the theoretical line (i.e., n versus n).

The results depicted in Figures 8 and Figure 9, together with the corresponding information given in Table 1, suggest that the proposed CRO-based amplitude measurement method, combined with a parallel resonant BPF, is an excellent laboratory activity for students, achievable using only simple circuitry and their smartphone camera.

Estimating the value of the number π:

The modern symbolic depiction of the Greek letter π in scientific literature appears as a constant number, generally approximated as 3.14159. It is widely accepted in the scientific community as an irrational and transcendental number, often associated with the ratio obtained by dividing the circumference of a circle by its diameter. Historically, countless approaches with varying levels of complexity have been adopted to estimate π. The eighteenth century's William Jones and Leonhard Euler are famous for introducing the modern Greek symbol for π in the calculus era, following the work of Newton. The Fourier series is a powerful tool for the mathematical estimation of π. Other sources containing extensive information on π calculations are listed in the following references [12][13][14][15][16].

CRO screen snapshot method:

This section presents an innovative university-level laboratory experiment that can be used to estimate a numerical value of the number Pi (denoted by the famous Greek letter, π), as tabulated in the last column of the above Table 1. In brief, the proposed experiment involves the Fourier analysis of a square wave using a CRO and a resonant circuit. A BPF is used to isolate individual frequency components (i.e., the odd harmonics) of the square wave. The amplitudes of these odd harmonics can then be measured using the CRO, and the theoretical prediction of 1/n behavior (n = odd) can be tested.

As shown in Equation (7), the amplitudes are predicted to go as:

$$A_{n\,(\sin e)} = \frac{4V_{o\,(square)}}{n\pi} \text{ (for } n = \text{odd)}$$

If one considers the value of π as the "unknown," the measured amplitudes can be used to determine a numerical value for π as:

$$\pi = \frac{4V_{o\,(square)}}{n\,A_{n\,(\sin e)}} \quad (17)$$

Where Vo (square) = An (square) = 3 Volts was kept constant throughout the experiment.

A detailed quantitative error analysis of the results is presented below. The experimentally determined mean value of π, obtained from the last column (column 8) of Table 1 for six Fourier components (n = 1, 3, 5, 7, 9, 11), was 3.15873. The standard deviation was 0.056494, and the total uncertainty was 0.128430, corresponding to a relative uncertainty of approximately 4.07%. The total uncertainty combines the statistical uncertainty (standard error of the mean = 0.02306, ~0.73%) with the dominant systematic uncertainty, estimated at ±4%, arising from analog measurement limitations. These limitations include the combined effects of the CRO display resolution and, where applicable, manual box counting error. The error analysis shows that the total measurement precision is mainly constrained by systematic effects associated with instrumental and human reading accuracy, rather than by random variations between trials that are comparatively minor. Hence, improving accuracy requires reducing these systematic contributions—through modern instrumentation or improved measurement protocols—rather than merely increasing the number of trials. In addition, the relative percentage error compared to the accepted value of π (= 3.14159) was 0.546%, and the percent uncertainty was approximately 0.0003%. These results demonstrate that the BPF-based approach provides a statistically robust and reproducible method for approximating the value of number π (Pi).

Graphical Analysis Method:

The experimental data provided in Table 1 can be transferred to a computer for further data analysis using software (for example, Excel or Origin) in order to enhance the engagement of the laboratory activity. For instance, in the following, we suggest, similarly to above, a computer-generated graphical approach for the estimation of the number π. Let us rewrite Equation (7) such that:

$$\Rightarrow \frac{4V_{o\,(square)}}{A_{n\,(\sin e)}} = \pi n \quad (18)$$

In our experiment, the amplitude of the input square wave was kept constant throughout at Vo (square) = 3 Volts. Therefore, above Equation (18) becomes:

$$\frac{12}{A_{n\,(\sin e)}} = \pi n \text{ (for } n = \text{odd)} \quad (19)$$

Thus, by plotting Equation (18) or Equation (19) (i.e., using the data given in column 7 of Table 1), the slope of the numerically fitted data will yield the required value of the number π. The experimental results obtained using the above Equation (18) are plotted in Figure 10.

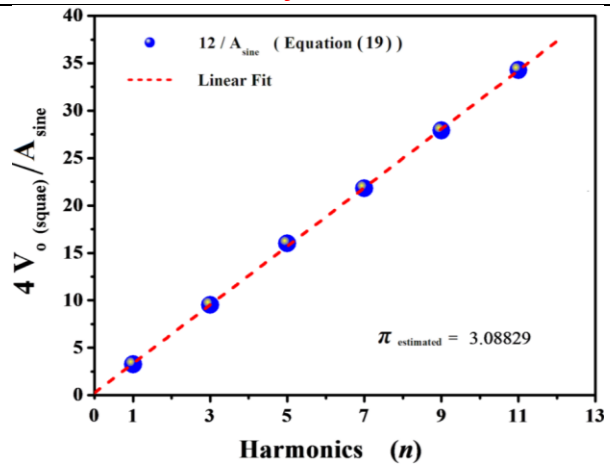

Figure 10. Proposed graphical method for the estimation of the value of number Pi (π). The experimental data are plotted according to equation (19). The dotted line represents a linear fit.

It should be noted that the value of the number Pi (π) obtained from computer-based graphical or linear regression analysis (see Figure 10) resulted was 3.08829, with a standard deviation of 0.179066 and an R-squared value of 0.999904. A comparison of this π value with the standard literature value of π (= 3.14159) resulted in an error of only 1.697% with a percent uncertainty value of approximately 0.0003%, thereby validating the linear fitting procedure. The computer-based linear fitting analysis method is quick, easy, and would permit students to explore further possibilities with this experiment.

Finally, between the two methods (CRO-based and Graphical analysis), a percent difference of 2.255% was observed with only 1.128% percent uncertainty, which reflects the total precision and reliability of the experimental methods used.

Broader scientific and Pedagogical Implications:

The parallel BPF circuit experiment offers valuable opportunities for integration into contemporary physics laboratories, demonstrating fundamental resonance and energy exchange concepts. The proposed experiments are highly scalable because varying the values of R, L, and C parameters, the number of cycles, or the damping rate allows systematic exploration of the circuit's frequency-dependent harmonic response, quality factor, and consequently the bandwidth. In fact, its scalable design allows adaptation from basic educational setups to advanced research applications. Introducing potential digital enhancements such as automated data acquisition, high-resolution oscilloscopes, and computational modeling can improve measurement precision, reproducibility, student engagement, and the overall pedagogical impact. We believe that, to the best of our knowledge, the proposed facile recipe to estimate the value of the number π is innovative and an exciting activity for the laboratory students.

Recommendations for Future Work:

To improve the precision and reproducibility of the BPF circuit experiments, future studies could incorporate digital oscilloscopes with higher sampling rates to conduct more detailed waveform analysis. Employing Arduino-based low-cost automated data acquisition systems would further improve experimental reliability and reproducibility. The use of optimized filtering techniques and higher-precision inductors and capacitors would reduce component tolerances, enhancing measurement accuracy. Additionally, computational modeling and simulation may complement laboratory work, allowing for the investigation of complex circuit configurations and resonance phenomena.

Conclusions: We demonstrated experimental investigations of the basic principles of the Fourier series using a simple parallel resonant band-pass filter (BPF) driven by a periodic

square wave and observed via an oscilloscope. This was achieved by generating Fourier components on the CRO screen, and measuring their amplitudes either by counting the number of square boxes directly or using an image captured by a digital or smartphone cameraartphone's camera). In fact, the captured images enhance the precise readability of the amplitudes when combined with the zooming function. Here, the BPF circuit is exposed as a remarkable Fourier analyzer tool, used to separate individual frequency components (i.e., the odd harmonics) of the applied square wave. These amplitudes and corresponding square wave frequencies can then be easily compared with the theoretical prediction of 1/n behaviour (n = odd), making exciting experimentation for the students in the laboratory. We then indicated how the exploration of such a simple BPF can be extended to extract the value of the famous number Pi (π). Due to its simplicity, this activity is well-suited for laboratory demonstrations of resonance BPF circuits, harmonics, and Fourier analysis that can provide students with exposure to the emerging fields of applied physics and electronics. We have presented the measurements and calculations clearly and elegantly.

Acknowledgement:

All authors would like to thank the Department of Physics, University of the Punjab, Lahore-54590, Pakistan.

Author Contributions:

Author MR served as principal investigator, conceptualized the study, designed and carried out the experiments, and also prepared the initial draft. Authors HW and HM assisted in experimental measurements, theoretical analysis, and data interpretation. All authors contributed to discussions and approved the final manuscript.

Conflict of Interest:

The Authors declare that they have no conflict of interest in publishing this manuscript in IJIST.

References:

[1] "Principles of Fourier Analysis - 2nd Edition - Kenneth B. Howell - Rou." Accessed: Mar. 09, 2026. [Online]. Available: https://www.routledge.com/Principles-of-Fourier-Analysis/Howell/p/book/9781032477008

[2] C. J. Pereyra, M. Osorio, A. Laguarda, and D. L. Gau, "Fourier analysis of a vibrating string through a low-cost experimental setup and a smartphone," *Phys. Educ.*, vol. 53, no. 4, p. 045019, Jun. 2018, doi: 10.1088/1361-6552/aac488.

[3] I. Singh and B. Kaur, "Teaching graphical simulations of Fourier series expansion of some periodic waves using spreadsheets," *Phys. Educ.*, vol. 53, no. 3, p. 035031, Apr. 2018, doi: 10.1088/1361-6552/aab447.

[4] M. T. Caccamo, G. Castorina, F. Catalano, and S. Magazù, "Rüchardt's experiment treated by Fourier transform," *Eur. J. Phys.*, vol. 40, no. 2, p. 025703, Jan. 2019, doi: 10.1088/1361-6404/aaf66c.

[5] Peter F. Hinrichsen, "Fourier analysis of the non-linear pendulum," *Am. J. Phys*, vol. 88, no. 12, pp. 1068–1074, 2020, doi: https://doi.org/10.1119/10.0001788.

[6] P. Ashdhir, J. Arya, C. E. Rani, and Anshika, "Exploring the fundamentals of fast Fourier transform technique and its elementary applications in physics," *Eur. J. Phys.*, vol. 42, no. 6, p. 065805, Sep. 2021, doi: 10.1088/1361-6404/ac20ad.

[7] V. L. B. De Jesus, C. Haubrichs, A. L. De Oliveira, and D. G. G. Sasaki, "Video analysis of a massive coiled spring transverse oscillations described by Fourier series," *Eur. J. Phys.*, vol. 43, no. 6, p. 065001, Aug. 2022, doi: 10.1088/1361-6404/ac831f.

[8] M. Riaz, "An exhibition of a rich variety of periodic attractors through alternation in elemental order of series LCR-type resonant circuits," *Eur. Phys. J. Plus 2020 1356*, vol. 135, no. 6, pp. 498-, Jun. 2020, doi: 10.1140/epjp/s13360-020-00521-6.

[9] Josué Lara-Reyes, Mario Ponce-Silva, "Series RLC Resonant Circuit Used as

Frequency Multiplier," *Energies*, vol. 15, no. 24, p. 9334, 2022, doi: https://doi.org/10.3390/en15249334.

[10] M. Riaz, "A remarkably facile automated numerical data extraction tool from oscilloscope screen snapshots," *Eur. J. Phys.*, vol. 41, no. 6, p. 065806, Oct. 2020, doi: 10.1088/1361-6404/aba4db.

[11] Rod Cross, "A simple method to estimate Q for a damped oscillation," *Phys. Teach*, vol. 62, no. 5, p. 406, 2024, doi: https://doi.org/10.1119/5.0208143.

[12] T. Williamson, "Calculating Pi Using the Monte Carlo Method," *Phys. Teach.*, vol. 51, no. 8, pp. 468–469, Nov. 2013, doi: 10.1119/1.4824938.

[13] R. O. Ocaya, "Estimating π using an electrical circuit," *Eur. J. Phys.*, vol. 38, no. 1, p. 015803, Nov. 2016, doi: 10.1088/0143-0807/38/1/015803.

[14] U. B. Pili, "Rapid estimation of π by weighing triangles, circles, and ellipses," *Phys. Educ.*, vol. 57, no. 2, p. 025025, Jan. 2022, doi: 10.1088/1361-6552/ac45c8.

[15] Vibhooti Shekhawat, "Graphite-paper circuit elements: Resistor, capacitor, and π value estimation," *Phys. Teach*, vol. 61, no. 2, pp. 154–155, 2023, doi: https://doi.org/10.1119/5.0077435.

[16] K. I. Nagao, Y. Sakano, T. Shinohara, Y. Matsuda, and H. Takami, "Estimation of π via experiment," *Eur. J. Phys.*, vol. 46, no. 4, p. 045006, Jul. 2025, doi: 10.1088/1361-6404/adebc0.